Chinese Chemical Letters 32 (2021) 2047–2051

Contents lists available at ScienceDirect

Chinese Chemical Letters

journal homepage: www.elsevier.com/locate/cclet

Communication

Fabrication of HRP/Bi_2WO_6 photoenzyme-coupled artificial catalytic system for efficiently degrading bisphenol A

Hongjun Dong[a], Ning Song[a], Ming Yan[a], Huihui Wu[a], Haibo Zhang[a], Changchang Ma[b], Yun Wang[a,*]

[a] *Advanced Chemical Engineering Laboratory of Green Materials and Energy of Jiangsu Province, Institute of Green Chemistry and Chemical Technology, School of Chemistry and Chemical Engineering, Jiangsu University, Zhenjiang 212013, China*
[b] *Department of Chemistry, Dongguk University, Seoul 04620, Republic of Korea*

ARTICLE INFO

Article history:
Received 14 September 2020
Received in revised form 15 October 2020
Accepted 9 November 2020
Available online 10 November 2020

Keywords:
Photoenzyme-coupled
Bi_2WO_6/HRP
Synergistic catalytic effect
BPA degradation
Reaction mechanism

ABSTRACT

A novel photoenzyme-coupled artificial catalytic system is fabricated by immobilizing horseradish peroxidase (HRP) on the Bi_2WO_6 hollow nanospheres *via* a facile electrostatic self-assembly process. The obtained Bi_2WO_6/HRP sample not only improves the visible light harvest ability but also promotes the high-efficiency separation of charge carriers. More importantly, the photogenerated electrons and produced H_2O_2 on Bi_2WO_6 directly take part in redox cycle reactions of HRP to induce photoenzyme synergic catalytic effect. In consequence, the degradation activity of Bi_2WO_6/HRP is significantly improved relative to Bi_2WO_6 and HRP for removing bisphenol A (BPA) under the visible light irradiation. This work launches a feasible design strategy for exploiting photoenzyme-coupled artificial catalytic system with special structure to degrade organic pollutants in water efficiently.

Organic wastewater pollution caused by industrial development has become increasingly severe so as to affect the survival of organisms and human health [1–4]. Up to now, many efforts have focused on reducing the harm caused by organic pollutants in wastewater by developing the photocatalysis and biocatalysis technologies. It is well known that the solar-driven photocatalysis process has the features of stable performance and no secondary pollution [5–9] and the biocatalysis process exhibits the high degradation efficiency and mild operating conditions [10]. Recently, fabricating photoenzyme-coupled artificial catalytic system has been regarded as novel potential promising strategy because it can produce synergistic catalytic effect between photocatalysis and biocatalysis, which has lately been evidenced as the effective heterogeneous catalytic reaction for organic pollutant degradation [11]. For instance, we prepared a photocatalyst/enzyme heterojunction *via* immobilizing horseradish peroxidase (HRP) on the surface of mesoporous graphitic carbon nitride [12], which exhibits the outstanding degradation activity and cycle stability for removing bisphenol A (BPA) in water. Zhang, *et al.* also fabricated integrated TiO_2-HRP hybrid catalyst, which exhibited the prominent catalytic performance, reusability and thermostability for the degradation of 2,4-dichlorophenol [13]. Therefore, fabricating photoenzyme-coupled artificial catalytic system has been expected to achieve high-efficiency catalytic performance for degrading the organic pollutants in water.

For immobilizing bio-enzyme on the photocatalyst surface to hold the enduring activity and stability, photocatalyst should meet a variety of conditions, such as low toxicity, fine biological compatibility, high chemical stability, *etc*. [14]. As one of the most attractive visible-light driven photocatalysts for degrading organic pollutants, Bi_2WO_6 has the superior intrinsic properties, such as unique layered structure, suitable energy band positions, high photothermal chemical stability and low toxicity [15–19]. More importantly, it is active for water oxidation to $^{\bullet}OH$ and H_2O_2 under visible light irradiation, and H_2O_2 can act as accessory ingredient of enzyme catalytic reaction [20]. Therefore, Bi_2WO_6 can serve as an ideal candidate for immobilization of enzyme to fabricate the photoenzyme-coupled artificial catalytic system. It is reported that the Bi_2WO_6 hollow microsphere exhibits some obvious advantages owing to its unique hierarchical architecture composed of thin nanosheets [21]. For instance, it exhibits large specific surface area and outstanding permeation features, which is conducive to enzyme passing through surface abundant pore channels to complete inside and outside immobilization. Meanwhile, the thin Bi_2WO_6 nanosheet structure can generate a synergy of accommodating the volume swing and promoting the transport and

* Corresponding author.
E-mail address: yunwang@ujs.edu.cn (Y. Wang).

https://doi.org/10.1016/j.cclet.2020.11.015

separation of charge carriers [21]. Therefore, the Bi_2WO_6 hollow microsphere avails to induce the photoenzyme-coupled synergistic catalytic effect.

Herein, a novel photoenzyme-coupled artificial catalytic system was constructed based on HRP and Bi_2WO_6 hollow microspheres, in which the HRP was immobilized on the internal and external Bi_2WO_6 hollow microsphere. The as-prepared Bi_2WO_6/HRP sample distinctly improves visible light response ability and the separation efficiency of charge carriers, finally realizing the high-efficiency degradation of BPA in water.

As X-ray diffraction (XRD) shown in Fig. 1a, the intense and sharp diffraction peaks of Bi_2WO_6 sample are produced, implying the identical crystalline phase Bi_2WO_6 with good crystallinity is obtained (JCPDS Card No. 73-1126) [22]. No diffraction peaks of HRP are appeared in XRD of Bi_2WO_6/HRP-2 sample, which is probably due to the trace loading. Moreover, scanning electron microscopy (SEM) image (Fig. 1b) exhibits that the Bi_2WO_6 sample has the high-uniform dispersion and the individual microsphere has a diameter of about 5 μm. The abundant pores are formed on Bi_2WO_6 sample owing to assembly of nanosheets, which can act as the transport channels in favor of enzymes and pollutant molecules diffusing into the hollow microsphere. It will enhance the immobilization of HRP on Bi_2WO_6 to improve the degradation activity and stability. In addition, the SEM image (Fig. 1c) shows the remained hollow microsphere architecture of Bi_2WO_6 after immobilizing HRP. Furthermore, as transmission electron microscopy (TEM) image spotted in Fig. 1d, the obvious brightness difference between edge and center of individual Bi_2WO_6 microsphere confirms the hollow structure feature. Besides, TEM image (Fig. 1e) further reveals that Bi_2WO_6 microsphere is assembled by thin nanosheets with thicknesses of about 14 nm. The thin nanosheet architectural feature can shorten the charge transfer distance perpendicular to nanosheet planes to improve the separation efficiency of charge carriers. High resolution TEM (HRTEM) image (Fig. 1f) shows the distinct lattice fringes with an interplanar spacing of 0.272 and 0.315 nm, which agrees well with the (002) and (131) lattice planes of Bi_2WO_6, respectively [23]. Moreover, For TEM image of Bi_2WO_6/HRP-2 sample shown in Fig. 1g, HRP is anchored on the external and interior of Bi_2WO_6 hollow microsphere, which is also apparently confirmed by bright and fluorescence field images of laser scanning confocal microscope (LSCM) in Figs. 1h and i. The results above demonstrate the formation of Bi_2WO_6/HRP photoenzyme-coupled artificial catalytic system.

The photocatalytic activity of samples was evaluated by the degradation of BPA under the visible light irradiation. Firstly, we confirm that the Bi_2WO_6/HRP-2 sample has the optimal photodegradation performance when the mass fraction of HRP is 2% (Fig. S1 in supporting information). The degradation dynamic curves of BPA in Fig. 2a indicate that only 3% and 45.6% BPA is degraded over the HRP and Bi_2WO_6 sample within 90 min, respectively. In contrast, the degradation rate of BPA over the Bi_2WO_6/HRP-2 sample reaches up to 84.5%. Besides, the degradation kinetic curves of BPA can be approximated as a *pseudo*-first-order process and the plots of $\ln(C_0/C)$ *versus* time are depicted in Fig. 2b, the fitting degradation rate constant of BPA over the Bi_2WO_6/HRP-2 (0.0193 min^{-1}) is 2.8 and 64 times larger than that of Bi_2WO_6 (0.0070 min^{-1}) and HRP (0.00003 min^{-1}), respectively. Meanwhile, Fig. 2c displays that the absorbance of BPA solution gradually decreases with the degradation progression, forecasting that the benzene ring structure is completely decomposed into small molecule/ion products [24]. Moreover, the degradation rate of BPA (Fig. 2d) is still as high as 78.6% and the relative enzyme activity can maintain 55.9% after four cycles (Fig. S2 in Supporting information), indicating that the Bi_2WO_6/HRP-2 sample has the superior stability and recyclability.

Moreover, the possible produced intermediates are inferred by MS in the BPA degradation process. As shown in Fig. S3a

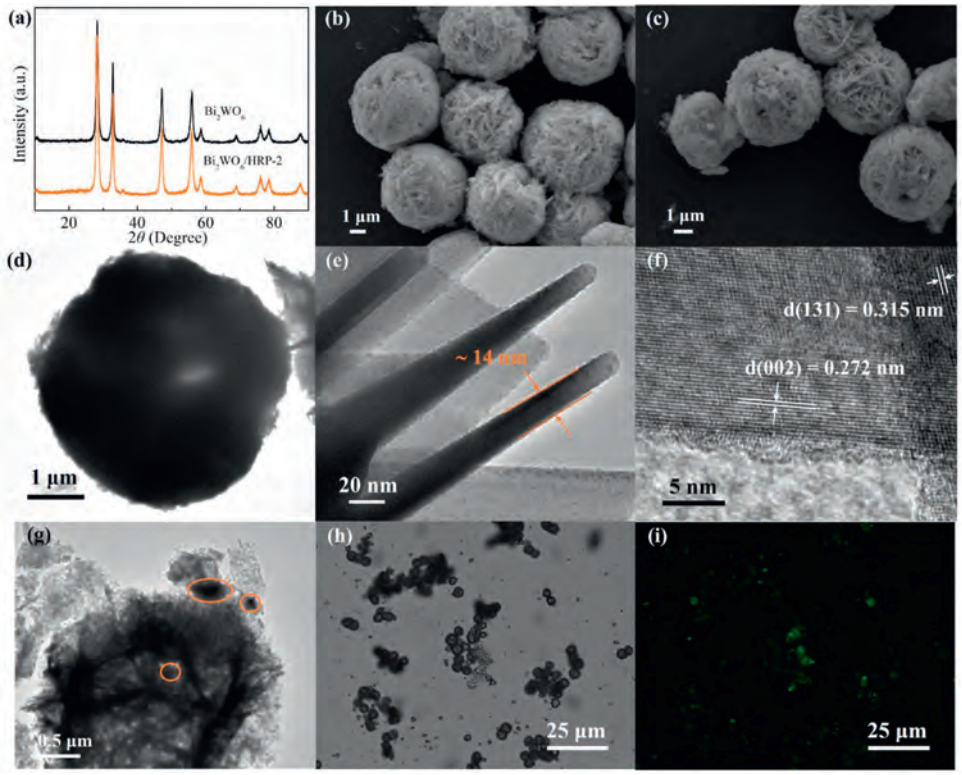

Fig. 1. XRD patterns of Bi_2WO_6 and Bi_2WO_6/HRP-2 (a). SEM images of Bi_2WO_6 (b) and Bi_2WO_6/HRP-2 (c). TEM (d, e) and HRTEM (f) images of Bi_2WO_6. TEM (g), LSCM bright field (h) and fluorescence field (i) images of Bi_2WO_6/HRP-2.

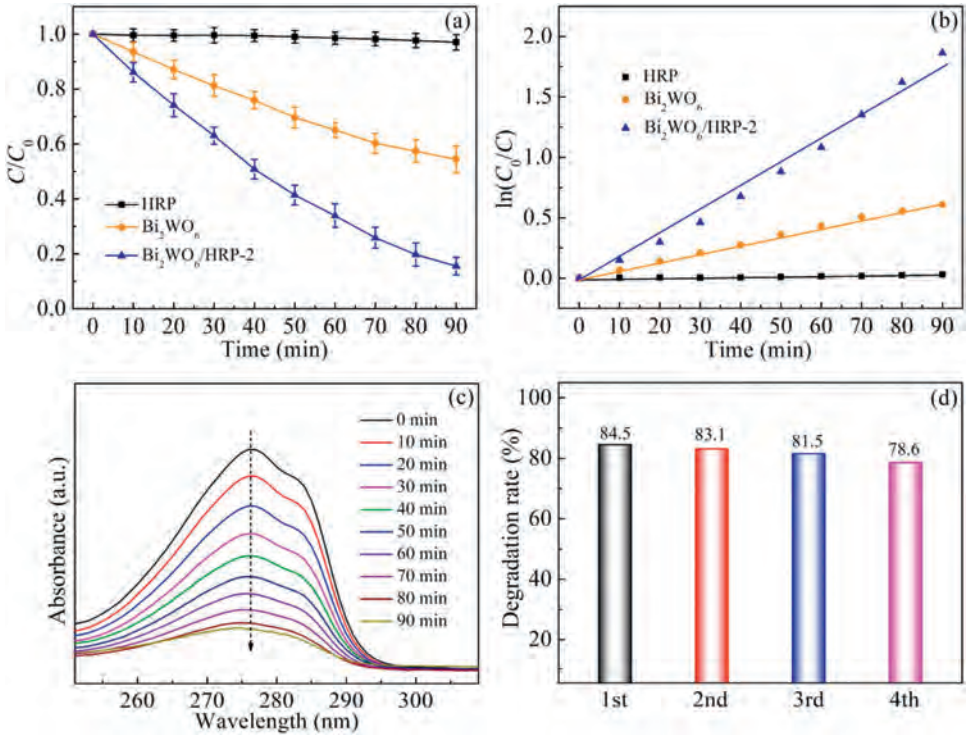

Fig. 2. Degradation dynamic curves (a) and plots of ln(C_0/C) *versus* time (b) of BPA solution over HRP, Bi_2WO_6 and Bi_2WO_6/HRP-2. Absorbance variation (c) and cycle degradation dynamic curves (d) of BPA over Bi_2WO_6/HRP-2.

(Supporting information), a strong signal is observed at *m/z* 277 owing to releasing H^+ from one phenolic hydroxyl group of BPA. After 60 min of degradation reaction, Fig. S3b (Supporting information) shows that the signal intensity at *m/z* 277 decreases significantly and some new signals appeared at the low *m/z* values, where compound **A** is decomposed into **B** (*m/z* 207), **C** (*m/z* 188) and **D** (*m/z* 149) by the ring-opening reaction of one benzene ring. And then compounds **B**, **C** and **D** are further degraded to **E** (*m/z* 127), **F** (*m/z* 116) and **G** (*m/z* 110) through breaking long side chains and opening the double bonds in the benzene ring. Subsequently, compounds **E**, **F** and **G** further take place the ring-opening reaction to produce H (*m/z* 131) and I (*m/z* 62), finally

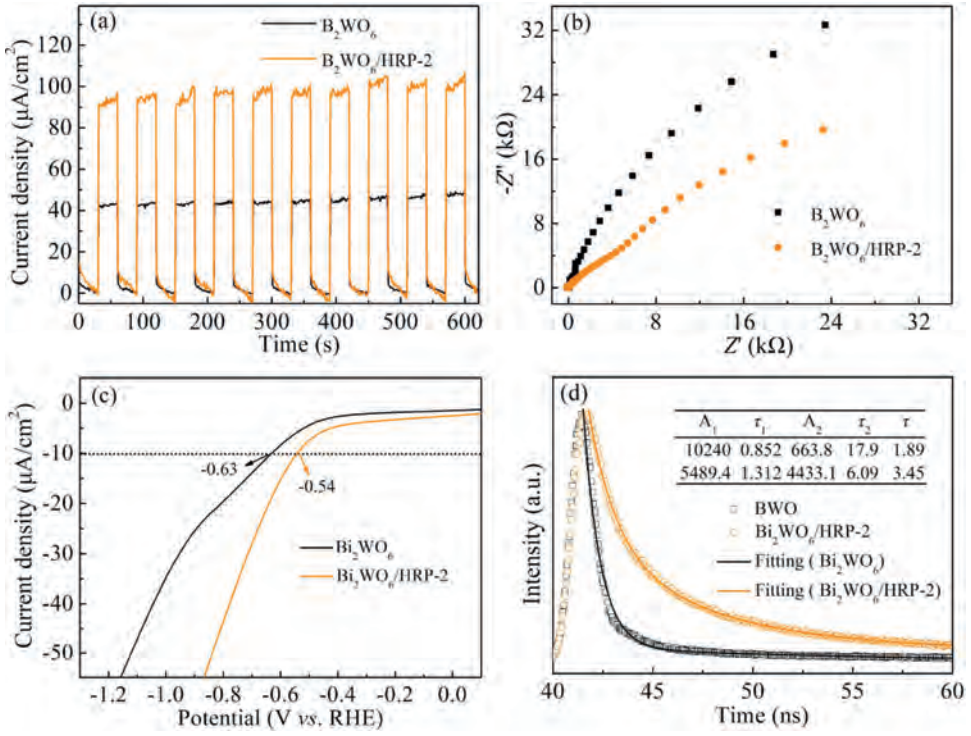

Fig. 3. Transient photocurrent responses (a), EIS Nyquist plots (b), polarization curves (c) and TR-PL decay curves (d) of Bi_2WO_6 and Bi_2WO_6/HRP-2.

being decomposed into CO_2 and H_2O. When the degradation reaction prolongs to 90 min, all signal intensities in Fig. S3c (Supporting information) further decrease distinctly, which implies all the produced intermediates can be degraded and mineralized. Based on these analyses, the possible degradation intermediates and pathway of BPA are shown in Fig. S4 (Supporting information).

The optical absorption property of the samples is investigated *via* Uv–vis diffuse reflectance spectrum (UV–vis DRS) (Fig. S5 in Supporting information) [25]. The Bi_2WO_6/HRP-2 sample displays a slight red-shift of absorption edge and produces the obvious absorption in excess of 450 nm, which is in favor of the solar harvest and utilization. In addition, the band gap energy of Bi_2WO_6 decreases from 2.63 eV to 2.53 eV after immobilizing HRP, which suggests electrons are more easily excited from valence band (VB) to conduction band (CB) to enhance the photocatalytic activity. Meanwhile, the VB values of Bi_2WO_6 before and after immobilizing HRP can be calculated to be 3.02 eV and 2.97 eV, while corresponding CB values are 0.39 eV and 0.44 eV, respectively. Moreover, it is reported that photocurrent and electrochemical impedance spectroscopy (EIS) reflect the migration and separation ability of photogenerated electron-hole pairs [26–28]. As shown in Fig. 3a, the photocurrent intensity of the Bi_2WO_6/HRP-2 electrode is far higher than that of Bi_2WO_6, which indicates that the incorporation of HRP distinctly improves the interfacial charge separation efficiency and mobility. The Nyquist curve radius of the Bi_2WO_6/HRP-2 electrode is clearly smaller than that of Bi_2WO_6 (Fig. 3b), suggesting that the former possesses the lower charge migration resistance in interfacial electrolyte solution, in favor of enhancing photocatalytic degradation activity. Furthermore, as polarization curves shown in Fig. 3c, the overpotential of Bi_2WO_6/HRP-2 electrode (−0.54 V) at 10 mA/cm^2 is distinctly smaller than that of Bi_2WO_6 (−0.63 V), which demonstrates that the incorporation of HRP effectively decreases the overpotential and thus fundamentally improves the photocatalytic degradation activity [29,30]. Moreover, based on the time-resolved photoluminescence (TR-PL) decay plots (Fig. 3d), the fitted fluorescence lifetime (1.89 ns) of Bi_2WO_6/HRP-2 sample is obviously shorter than that of Bi_2WO_6 (3.45 ns), which implies that the probable new nonradioactive decay way is produced to suppress recombination of photogenerated electrons and holes [31,32]. These results indicate that the immobilization HRP on Bi_2WO_6 microsphere has a positive effect to improve the photocatalytic activity. Besides, the similar pore structure and specific surface areas of the Bi_2WO_6 and Bi_2WO_6/HRP-2 samples (Fig. S6 in Supporting information) imply that they have insignificant effect on the photocatalytic activity, indirectly attesting that the enhanced degradation activity mainly originates from the photoenzyme synergic catalytic effect produced on the Bi_2WO_6/HRP-2 sample.

Triethanolamine (TEOA), ascorbic acid (AA) and isopropanol (IPA) act as scavengers of holes (h^+), superoxide radical ($O_2^{\bullet-}$) and hydroxyl radical ($^{\bullet}OH$) to investigate the photocatalytic degradation mechanism of BPA, respectively. As depicted in Fig. 4a, when TEOA and AA are added to the reaction system, the degradation rate of BPA decreases from blank 84.5%–23.3% and 38.6%, respectively. The strong inhibition effect manifests that h^+ and $O_2^{\bullet-}$ are major active species involved in degradation reaction. In addition, the degradation rate of BPA also decreases to 64.2% in the presence of IPA, suggesting that $^{\bullet}OH$ also plays an important role. Moreover, the generated $O_2^{\bullet-}$ and $^{\bullet}OH$ active species are further detected by ESR spectra (Figs. 4b and c), in which the strong characteristic signals can be observed under the visible light illumination, further declaring $O_2^{\bullet-}$ and $^{\bullet}OH$ active species are produced in the BPA degradation process

On the base of discussions above, we propose the possible photoenzyme synergistic catalytic mechanism over the Bi_2WO_6/HRP sample in Fig. 4d. The photogenerated electrons and holes are firstly produced on the Bi_2WO_6/HRP sample and migrate to the surface under the visible light irradiation, respectively. It is reported that the one-electron reduction of O_2 by electron on

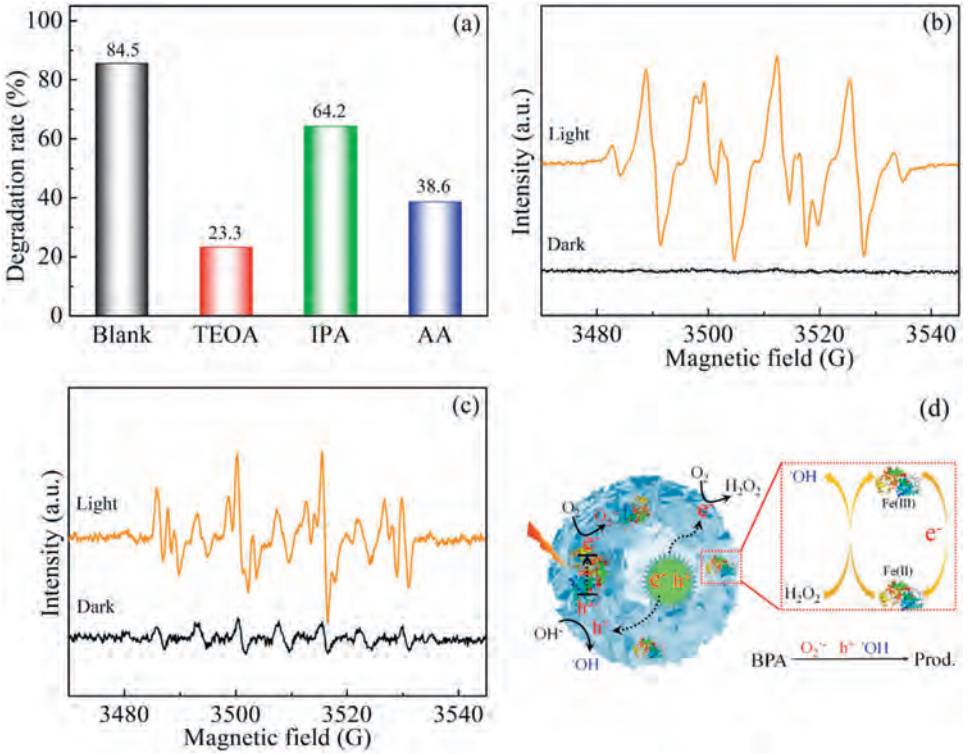

Fig. 4. Degradation rate of BPA over Bi_2WO_6/HRP-2 with different capture agents (a), ESR spectra in the methanol dispersion for DMPO-$O_2^{\bullet-}$ (b) and in the aqueous dispersion for DMPO-$^{\bullet}OH$ (c), possible degradation mechanism diagram (d).

Bi_2WO_6 is not allowed in thermodynamics because the CB position (0.44 eV) of Bi_2WO_6 is more positive than reduction potential of $O_2/O_2^{\bullet-}$ (−0.046 V *vs.* NHE), but the multiple electron reduction of O_2 can be occurred easily owing to the more positive reduction potential of O_2/H_2O_2 (−0.70 V *vs.* NHE) [20]. Therefore, the photogenerated electrons reduce O_2 dissolved in water to produce H_2O_2 and $O_2^{\bullet-}$ on Bi_2WO_6 and HPR, respectively. Notably, Fe^{3+}-porphyrin (oxidized state) in HRP can be reduced by photogenerated electrons to transform into reduction state, and H_2O_2 can oxidize Fe^{2+}-porphyrin (reduction state) to recover oxidation state simultaneously and produce $^{\bullet}OH$. As a result, $^{\bullet}OH$ is released continuously, which significantly improves the degradation performance. Meanwhile, $^{\bullet}OH$ can also be produced by reaction between h^+ and OH^- because the standard redox potential of $OH^-/^{\bullet}OH$ (2.3 V *vs.* NHE) is higher than VB position of Bi_2WO_6 (2.97 eV). Finally, hole, $^{\bullet}OH$, and $O_2^{\bullet-}$ active species further oxidize BPA to CO_2 and H_2O. We have to point out that the Bi_2WO_6 hollow structure avails immobilization of HRP and diffusion of BPA molecule in and out of microsphere through the abundant pore channels, promoting the photoenzyme synergistic catalytic effect to improve degradation performance for removing BPA.

In summary, a photoenzyme-coupled artificial catalytic system Bi_2WO_6/HRP is prepared, in which HRP significantly enhances the visible light absorption ability and separation efficiency of charge carriers, in favor of improving the catalytic degradation activity. The optimal degradation rate constant of BPA over the Bi_2WO_6/HRP-2 sample reaches up to 0.0193 min^{-1}, which is 2.8 and 64 times larger than that of Bi_2WO_6 (0.0070 min^{-1}) and HRP (0.00003 min^{-1}), respectively. The photocatalytic degradation mechanism indicates that h^+, $^{\bullet}OH$ and $O_2^{\bullet-}$ all play the important roles in the process of degrading BPA, as well as the photogenerated electrons and produced H_2O_2 on Bi_2WO_6 can take part in the redox process of HRP to induce photoenzyme synergistic catalytic effect that results in the continuous release of ·OH to improve the catalytic degradation performance.

Declaration of competing interest

The authors declare that they have no known competing financial interests or personal relationships that could have appeared to influence the work reported in this paper.

Acknowledgments

This work was supported by the NSFC-Shanxi Coal Based Low Carbon Joint Fund (No. U1810117), the National Natural Science Foundation of China (No. 52072153), the Natural Science Foundation of Jiangsu Province (No. BK20190867), the Open Project Program of Key Laboratory of Preparation and Application of Environmental Friendly Materials (Jilin Normal University) (No. 2019009), the Open Project Program of Key Laboratory of Groundwater Resources and Environment (Jilin University), Ministry of Education (No. 202005001KF), and the Young Talent Cultivate Programme of Jiangsu University (No. 4111310017).

Appendix A. Supplementary data

Supplementary material related to this article can be found, in the online version, at doi:https://doi.org/10.1016/j.cclet.2020.11.015.

References

[1] S. Hu, Y. Yu, Y. Guan, et al., Chin. Chem. Lett. 31 (2020) 2839–2842.
[2] R. Mu, Y. Ao, T. Wu, C. Wang, P. Wang, J. Hazard. Mater. 382 (2020) 121083.
[3] A. Xie, J. Cui, J. Yang, et al., Appl. Catal. B: Environ. 264 (2020) 118548.
[4] L. Jing, Y. Xu, M. Xie, et al., Chem. Eng. J. 360 (2019) 1601–1612.
[5] Y. Xiao, Z. Peng, W. Zhang, Y. Jiang, L. Ni, Appl. Surf. Sci. 494 (2019) 519–531.
[6] M. Ren, Y. Ao, P. Wang, C. Wang, Chem. Eng. J. 378 (2019) 122122.
[7] Q. Wang, D. Astruc, Chem. Rev. 120 (2020) 1438–1511.
[8] M. Zhang, J. He, Y. Chen, et al., Chin. Chem. Lett. 31 (2020) 2721–2724.
[9] H. Dong, X. Zhang, J. Li, et al., Appl. Catal. B: Environ. 263 (2020) 118270.
[10] R. Zhang, L. Wang, J. Han, et al., J. Hazard. Mater. 383 (2020) 121130.
[11] H. Wang, W. Yang, X. Wang, et al., Sensor. Actuat. B: Chem. 304 (2020) 127389.
[12] H. Zhang, J. Wu, J. Han, et al., Chem. Eng. J. 385 (2020) 123764.
[13] X. Ji, Z. Su, M. Xu, G. Ma, S. Zhang, ACS Sustain. Chem. Eng. 4 (2016) 3634–3640.
[14] L. Wang, W. Zhi, D. Lian, et al., ACS Sustain. Chem. Eng. 7 (2019) 14611–14620.
[15] C. Li, G. Chen, J. Sun, et al., Appl. Catal. B: Environ 188 (2016) 39–47.
[16] J. Hu, D. Chen, Z. Mo, et al., Angew. Chem. Int. Ed. 58 (2019) 2073–2077.
[17] S. Cao, B. Shen, T. Tong, J. Fu, J. Yu, Adv. Funct. Mater. 28 (2018) 1800136.
[18] H. Shen, G. Liu, Y. Zhao, et al., Fuel 259 (2020) 1163119.
[19] H. Zhang, J. He, C. Zhai, M. Zhu, Chin. Chem. Lett. 30 (2019) 2338–2342.
[20] J. Sheng, X. Li, Y. Xu, ACS Catal. 4 (2014) 732–737.
[21] C. Li, G. Chen, J. Sun, et al., New J. Chem. 39 (2015) 4384–4390.
[22] T. Fei, L. Yu, Z. Liu, et al., J. Colloid Interf. Sci. 557 (2019) 498–505.
[23] X. Kong, T. Tong, B. Ng, et al., ACS Appl. Mater. Interfaces 12 (2020) 26991–27000.
[24] E. Jiang, N. Song, G. Che, et al., Chem. Eng. J. 399 (2020) 125721.
[25] R. Koutavarapu, B. Babu, C.V. Reddy, et al., J. Environ. Manage. 265 (2020) 110504.
[26] H. Liu, L. Li, C. Guo, et al., Chem. Eng. J. 385 (2020) 123929.
[27] H. Wang, J. Zhang, P. Wang, et al., Chin. Chem. Lett. 31 (2020) 2789–2794.
[28] D. Samanta, P. Basnet, T.I. Chanu, S. Chatterjee, J. Alloys Compd. 844 (2020) 155810.
[29] H. Dong, S. Hong, P. Zhang, et al., Chem. Eng. J. 395 (2020) 125150.
[30] H. Dong, M. Xiao, S. Yu, et al., ACS Catal. 10 (2020) 458–462.
[31] W. Tu, Y. Zhou, Q. Liu, et al., Adv. Funct. Mater. 23 (2013) 1743–1749.
[32] Y. Chen, J.F. Li, P.Y. Liao, et al., Chin. Chem. Lett. 31 (2020) 1516–1519.